




Cite this: *J. Anal. At. Spectrom.*, 2023, **38**, 758

# Characterizing a nitrogen microwave inductively coupled atmospheric-pressure plasma ion source for element mass spectrometry†

Monique Kuonen,  Guanghui Niu,  Bodo Hattendorf \* and Detlef Günther 

A high-power nitrogen-based microwave inductively coupled atmospheric-pressure plasma was coupled to a quadrupole mass spectrometer to investigate its characteristics as an ion source for element mass spectrometry. The influence of operating conditions on analyte sensitivity, plasma background, and polyatomic ion formation was investigated for conventional solution-based analysis. By varying the forward power and the nebulizer gas flow rate, the plasma background ions were found to decrease with increasing gas flow rates and decreasing operating power. Analyte ions showed different trends, which could be related to the physical–chemical properties of the elements. We could identify three groups based on the location of maximum intensity in the power vs. flow rate contour plot. Atomic ions of elements with low first ionization energy and low oxygen bond strength were found to maximize at a high nebulizer gas flow rate and lower microwave power. Elements with intermediate ionization energy and higher oxygen bond strength required higher power settings for optimum sensitivity, while elements with the highest ionization energies required the highest power and lowest gas flow rates for their optimization. The latter group showed a substantial suppression in sensitivity compared to elements of similar mass, which is considered to result from the high abundance of NO in the plasma source, whose ionization energy is close to that of these elements. Metal oxide ions were found at similar or higher abundances than in the conventional argon-based ICP and could be minimized only by using a low gas flow rate and high power settings. These general trends were also observed when the vacuum interface was modified. To change the dynamics of the supersonic expansion, different sampler cone orifice sizes and sampler–skimmer distances were investigated and the interface pressure was lowered through an additional pump. These modifications did not yield significant differences in ion transmission but lowering the interface pressure reduced the relative abundance of metal oxide ions. The limits of detection were evaluated for optimized plasma conditions and found comparable to those of an argon ICP source with the same mass spectrometer.

Received 14th November 2022  
Accepted 24th January 2023

DOI: 10.1039/d2ja00369d

rsc.li/jaas

## Introduction

Since its introduction<sup>1</sup> inductively coupled plasma mass spectrometry (ICPMS) has evolved over the past four decades into one of the most widely used lab-based and routine techniques for the chemical analysis of the elemental or isotopic composition of almost any sample type.<sup>2</sup> Its success is mostly due to its high sensitivity for most elements in the periodic table in particular though for metals, a wide linear dynamic range (up to 12 orders of magnitude),<sup>3</sup> and straightforward coupling to various sample introduction systems such as solution nebulization, laser ablation<sup>4,5</sup> and various separation techniques such

as high performance liquid chromatography and capillary electrophoresis.<sup>6–8</sup> While technological advancements were mainly focused on the mass spectrometer by optimizing ion transfer<sup>9,10</sup> and employing reaction cells<sup>11–13</sup> or different mass analysers,<sup>14–16</sup> the fundamental setup of the ion source<sup>17,18</sup> however has not undergone substantial changes within the last two decades. Even though different manufacturers of commercial instruments employ distinct configurations for the ICP, interface ion optics, and mass analysers, ICPMS has proven to be a reliable and robust analytical method.

Still, current instruments suffer from multiple drawbacks, such as the need for a complex power generator design, the occurrence of spectral interferences from Ar containing molecular ions, and the substantial running cost due to the consumption of up to 1 m<sup>3</sup> of Ar per hour in a common operating mode. Nitrogen-based plasma sources have been proposed as an alternative to the argon ICP decades ago.<sup>19,20</sup> Such microwave induced plasmas have also been described

Laboratory of Inorganic Chemistry, Department of Chemistry and Applied Biosciences, ETH Zurich, Vladimir-Prelog-Weg 1, Zurich 8093, Switzerland. E-mail: bodo@inorg.chem.ethz.ch

† Electronic supplementary information (ESI) available. See DOI: <https://doi.org/10.1039/d2ja00369d>



with elemental MS,<sup>21–23</sup> which however did not receive much attention. Most recently a new configuration of an inductively coupled microwave plasma source was introduced,<sup>24</sup> which can be operated with nitrogen as plasma gas while being capable of delivering a power of up to 1.5 kW, which compares favourably with common Ar ICPs. This novel microwave inductively coupled atmospheric pressure plasma (MICAP) has already been successfully employed as a plasma source for ICP optical emission spectrometry<sup>25</sup> and an initial study<sup>26</sup> using a prototype time-of-flight MS has revealed that with solution nebulization, the sensitivities were lower by a factor of two than those of an Ar ICP coupled to the same MS. Desolvation of the aerosol was found to enhance the sensitivity significantly and most recently solution nebulization and laser ablation sampling were employed with an ion source coupled to a quadrupole MS (QMS), where similar figures of merit to those obtained with an Ar ICP were obtained.<sup>27,28</sup> This study was aimed at investigating the characteristics of the new nitrogen-sustained plasma ion source coupled to a QMS with pneumatic nebulization. Therefore, the influence of forward power and the nebulizer gas flow rate was investigated to evaluate the analytical performance of the nitrogen microwave induced plasma (MIP). Since all the previous experiments used the vacuum interface and ion optic system designed for argon ICPMS instruments, various modifications of the interface arrangement were implemented to evaluate whether the gas dynamics at the vacuum interface or the ion optics could be optimized for the expansion dynamics of nitrogen versus argon plasmas.

## Experimental

### Instrumentation

The instrument prototype (Fig. 1) is based on a commercial ELAN 6100<sup>PLUS</sup> ICPMS (PerkinElmer, Canada), for which the conventional ICP has been replaced by a MICAP (Radom Corp, USA).<sup>24–26</sup> A cavity magnetron (1.5 kW Panasonic 2M262A-07AAM) generates a microwave field that is directed to a dielectric resonator ring and couples inductively to the plasma. The magnetron was powered by a Magdrive 2000 power supply (Dipolar AB, Sweden). A quartz disc between the MS vacuum interface and the torch protects the Teflon holder of the dielectric resonator from the heat of the plasma. A conventional Fassel-type quartz torch (Spectro Arcos SOP-Torch, 1.8 mm inner diameter injector, Spectro, Germany) was centred within the resonator ring with a 3D translation stage.

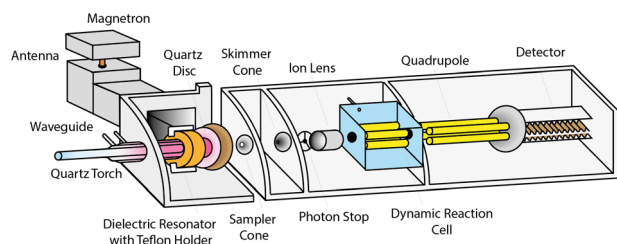


Fig. 1 Schematic depiction of the MICAP-MS.

The plasma ignition process as well as the operating parameters of the plasma were controlled through a MICAP control unit (Radom Corp., USA). During the start-up sequence, argon gas is introduced for 8 s together with nitrogen (99.996%, PanGas AG, Switzerland) simultaneously with a spark to facilitate the ignition. After the plasma ignition, no more argon is added, and the nitrogen-sustained plasma emits a pale-pink light.

The vacuum interface consisted of standard Elan-type sampler (1.1 mm orifice, platinum) and skimmer (0.8 mm, orifice platinum) cones, respectively. To investigate the supersonic expansion dynamics, the vacuum interface was modified. Different combinations of the sampler cone aperture, skimmer cone position, and interface pressure were studied: the sampler orifice diameter was decreased from 1.1 mm to 0.8 mm and the sampler-skimmer distance was shortened by introducing one or two 0.5 mm aluminium spacers at the base of the skimmer. Additionally, a second rotary vane pump (Leybold S25B) was employed to reduce the interface pressure. A pressure sensor (Pfeiffer Vacuum Single Gauge, Typ361) was connected to the vacuum line approximately 80 cm downstream of the interface to monitor changes in pressure for different configurations. The ion optics arrangement was not altered and a dynamic reaction cell was not employed in this study. The employed operating conditions of the instrument can be found in the ESI (Table S1†). The liquid sample was introduced with a glass concentric nebulizer (Micromist<sup>TM</sup> L90347) and a cyclonic spray chamber. The sample flow rate was controlled with a peristaltic pump, corresponding to 0.99 mL min<sup>-1</sup>. The sample uptake efficiency into the plasma was determined to be 3–5% of the sample flow rate, depending on the nebulizer gas flow rate.

### Materials and methods

A multi-element solution was prepared as 1 µg kg<sup>-1</sup> of each analyte by successive dilution with 1% nitric acid from single element stock solutions obtained from Merck (Na), Inorganic Ventures (Be, Mg, K, Ca, Co, Zn, Ge, As, Se, Rb, Sr, Cd, In, Cs, Te, Ba, Ce, Lu, Pb, Th, and U) and VWR Chemicals (Li) to investigate the influence of operating parameters and interface geometry on analyte sensitivity. The instrument was initially optimized for each interface configuration by adjusting the ion lens voltage and the torch position for maximum <sup>238</sup>U<sup>+</sup> intensity. For the optimization the plasma was operated at a power of 1350 W, with a cooling gas flow rate of 14 L min<sup>-1</sup>, a nebulizer gas flow rate of 1000 mL min<sup>-1</sup>, and an auxiliary gas flow rate of 750 mL min<sup>-1</sup>.

The influence of the operating conditions on analyte sensitivity was investigated by varying the operating power from 1150 W to 1450 W in steps of 100 W, while the nebulizer gas flow rate was increased from 800 mL min<sup>-1</sup> to 1100 mL min<sup>-1</sup> in steps of 50 mL min<sup>-1</sup>. The cooling and auxiliary gas flow rates remained fixed. The different interface configurations with which the measurement series were performed and how the operating conditions were varied are given in Table 1. For two interface configurations, only the gas flow rate was changed while the power remained at 1450 W. After each change in the



**Table 1** The different interface configurations for which the operating conditions were varied. The 1.1 mm sampler cone is a platinum cone, whereas the 0.8 mm one is made out of aluminium. Each aluminium spacer shifts the skimmer 0.5 mm further upstream. The power was varied in steps of 100 W, while the gas flow rate was set in steps of 50 mL min<sup>-1</sup>

| Interface configuration                       | Sampler aperture [mm] | Spacers | Additional pump | Power variation [W] | Flow variation [mL min <sup>-1</sup> ] |
|---|-----------------------|---------|-----------------|---------------------|--|
| Standard interface                            | 1.1                   | None    | No              | 1150–1450           | 800–1100                               |
| Reduced sampler                               | 0.8                   | None    | No              | 1150–1450           | 800–1100                               |
| Standard interface & pump                     | 1.1                   | None    | Yes             | 1150–1450           | 800–1100                               |
| 0.5 mm skimmer shift                          | 1.1                   | One     | No              | 1150–1450           | 800–1100                               |
| 1.0 mm skimmer shift                          | 1.1                   | Two     | No              | 1150–1450           | 800–1100                               |
| 0.5 mm skimmer shift & pump                   | 1.1                   | One     | Yes             | 1150–1450           | 800–1100                               |
| 1.0 mm skimmer shift & pump                   | 1.1                   | Two     | Yes             | 1150–1450           | 800–1100                               |
| 1.0 mm skimmer shift & reduced sampler        | 0.8                   | Two     | No              | 1450                | 800–1100                               |
| 1.0 mm skimmer shift & reduced sampler & pump | 0.8                   | Two     | Yes             | 1450                | 800–1100                               |

interface configuration or operating parameters, the ion lens voltages were re-calibrated. In addition to the analyte elements, the instrumental background at  $m/z$  220 and the plasma background ions  $^{15}\text{N}^+$ ,  $^{14}\text{N}^{16}\text{O}^+$ ,  $^{14}\text{N}_3^+$ , and  $^{14}\text{N}_4^+$  were monitored and the metal oxides  $^{140}\text{Ce}^{16}\text{O}^+$ ,  $^{232}\text{Th}^{16}\text{O}^+$ , and  $^{238}\text{U}^{16}\text{O}^+$  and their corresponding nitrides  $^{140}\text{Ce}^{14}\text{N}^+$ ,  $^{232}\text{Th}^{14}\text{N}^+$ , and  $^{238}\text{U}^{14}\text{N}^+$  were acquired. Each isotope was measured with a dwell time of 500 ms in one sweep and with 5 replicates.

To determine the limits of detection (LODs), a 1% nitric acid solution containing between 1 and 100  $\mu\text{g kg}^{-1}$  of the analytes in the Certipur® ICP multi-element standard solution VI from Merck was measured analogously after optimizing the instrument for maximum  $^{238}\text{U}^+$  signal intensity while keeping the  $^{140}\text{Ce}^{16}\text{O}^+$  abundance (expressed as  $^{140}\text{Ce}^{16}\text{O}^+ / (^{140}\text{Ce}^+ + ^{140}\text{Ce}^{16}\text{O}^+)$ ) below 3%. Additionally, the same solution was measured on a commercial Ar ELAN 6100<sup>PLUS</sup>.

### Data evaluation

Abundance corrected sensitivities for the analyte isotopes were calculated after subtracting the instrumental background signal. For the plasma background and molecular ion signals, only background subtraction was performed. The sensitivity of different analyte elements was analysed in dependence of forward power and nebulizer gas flow rates and trends were identified (*e.g.* oxide formation, sensitivity *etc.*). For visualization of the influence of forward power and nebulizer gas flow rates, the sensitivities were depicted in a contour plot for each analyte. The different interface configurations were compared using their response curves as well as their nitride and oxide ratios. For each configuration the operating conditions yielding the maximum achievable sensitivities while maintaining a  $^{140}\text{Ce}^{16}\text{O}^+$  abundance at or below 3% were determined. The LODs were determined from three times the standard deviation of the blank divided by the elements' blank-corrected sensitivities.

## Results and discussion

### Influence of operating conditions

The following discussion about the influence of the operating conditions is visualized with data from the standard interface &

pump configuration, which has been shown in preliminary experiments to be beneficial in terms of oxide abundance. However, the trends are representative for the other configurations, unless noted in the later section in which the interface modifications are discussed.

**Temperature and plasma potential.** Since the plasma gas temperature and the plasma potential correspond in a first approximation to the slope and the intercept of the optimum ion lens voltage in dependence of the mass,<sup>29</sup> the linear regression of the ion lens calibration can thus be used to infer changes in plasma temperature and potential. The variations of the slope and intercept however were found not to vary substantially to isolate clear trends. This was caused by the comparably wide ion transmittance peaks. Nonetheless, a general trend of a decreasing slope and intercept at higher nebulizer gas flow rates and with lower operating powers was observed (Fig. S1†), indicating that the gas temperature and plasma potential decrease accordingly. It is worth mentioning that the optimized lens voltages exhibited a lower intercept but a steeper slope when using the MICAP source than with the Ar ICP on the same instrument. Typical values for the Ar ICP are  $\approx 5$  V for the intercept and  $0.015$  V  $\text{amu}^{-1}$  for the slope. The lower intercept indicates that the plasma potential of the MICAP source is indeed lower as there is no potential gradient across the resonator. The steeper slope on the other hand indicates that the  $\text{N}_2$  plasma reaches a higher velocity during the expansion.

**Interface pressure.** Similar to the slope of the ion lens calibration, the interface pressure changes with the plasma's gas temperature.<sup>29</sup> The variation of interface pressure with nebulizer gas flow rates and forward powers is shown in Fig. S2† for the standard interface and when operating with an additional pump. In both cases, the interface pressure increases with increasing gas flow rate or decreasing operating power, which is due to a lower gas temperature. As a result of the inverse relationship between the interface pressure and the plasma gas temperature, the trend in plasma gas temperature is more pronounced than that from the lens calibration data. The change in gas temperature is thus about 2–4% per 100 mL min<sup>-1</sup> of the nebulizer gas flow for a constant power or



about 3% per 100 W of forward power for a constant gas flow rate.

**Analyte ion trends.** The analyte signal is dependent on ion transmission as well as the ionization efficiency of the ion source. The degree to which an element is ionized in turn depends on the ionization energy (IE) and the plasma conditions. To evaluate the dependence of the analyte signal on the first IE, elements with a similar mass and different first IEs were investigated ( $^{66}\text{Zn}^+$ ,  $^{72}\text{Ge}^+$ ,  $^{75}\text{As}^+$ ,  $^{80}\text{Se}^+$ ,  $^{85}\text{Rb}^+$ , and  $^{88}\text{Sr}^+$ ), whereas the sensitivities of the analytes at low gas flow rates (see Fig. S3†) can be attributed to their degrees of ionization – similar to those in an Ar ICP<sup>30</sup> – the sensitivities of elements with a low first IE increased with higher gas flow rates, which is most likely due to a more efficient ion sampling through the vacuum interface while those with high first IE decreased due to ionization suppression as the plasma temperature decreases with an increasing gas flow. A lower plasma temperature and the shorter residence time of the aerosol<sup>31</sup> at higher nebulizer gas flow rates decrease the analyte loss through radial diffusion in the source and thus increase the sampling efficiency.<sup>32</sup> Since diffusion is governed by the mobility of the ions and thus mass dependent, the dependence of the analyte sensitivity on the mass was studied for elements with similar first IEs and different masses. As shown in Fig. S4,† the sensitivities for elements with low first IE increased with the nebulizer gas flow rate but the degree of the increase varies with the analyte mass; lighter ions are more prone to diffuse and thus experience a stronger suppression at lower nebulizer gas flow rates.<sup>32</sup> On the other hand, elements with a higher IE suffered from the aforementioned ionization suppression, which explains the relative loss of  $^{66}\text{Zn}^+$ ,  $^{72}\text{Ge}^+$ ,  $^{75}\text{As}^+$  and  $^{80}\text{Se}^+$  relative to  $^{85}\text{Rb}^+$  when increasing the carrier gas flow (Fig. S3 right†) or decreasing the applied forward power. This relative suppression is a function of the elements' IE and mass, as  $^{75}\text{As}^+$  and  $^{80}\text{Se}^+$  appeared to be more suppressed than  $^{66}\text{Zn}^+$ , which is however due to a reduction of loss by diffusion of the lighter ions. For  $^{72}\text{Ge}^+$  both lower IE and higher mass caused the least relative suppression. This suppression can also be seen when ion pairs of similar mass and low vs. high IE are compared (see Fig. S5 right†). Increasing the gas flow rate led to stronger relative suppression of high IE elements and lighter high IE analyte ions

were less suppressed than heavier ones when normalized to the same low IE element (e.g.  $^{111}\text{Cd}^+ / ^{133}\text{Cs}^+$  vs.  $^{128}\text{Te}^+ / ^{133}\text{Cs}^+$ ).

For a better overview of these effects and the determination of operating conditions that yield the maximum sensitivity, the sensitivity dependence on forward power and nebulizer gas flow rate was depicted in a contour plot for every analyte. Three element groups can be identified based on the location of the maximum sensitivity, as seen in Fig. 2. The first group ( $^7\text{Li}$ ,  $^{23}\text{Na}$ ,  $^{24}\text{Mg}$ ,  $^{39}\text{K}$ ,  $^{85}\text{Rb}$ ,  $^{88}\text{Sr}$ ,  $^{115}\text{In}$ ,  $^{133}\text{Cs}$ ,  $^{137}\text{Ba}$ , and  $^{175}\text{Lu}$ ) is governed by elements with a low first IE, whose sensitivity increases with higher gas flow rates due to the higher sampling efficiency. Since many analytes in this group have a low mass, a higher operating power decreases the sensitivity through increased radial diffusion and possibly space charge effects at higher temperatures. The elements of the second group ( $^9\text{Be}$ ,  $^{59}\text{Co}$ ,  $^{72}\text{Ge}$ ,  $^{111}\text{Cd}$ ,  $^{140}\text{Ce}$ ,  $^{208}\text{Pb}$ ,  $^{232}\text{Th}$ , and  $^{238}\text{U}$ ) have intermediate first IEs or higher oxygen bond strengths<sup>33</sup> which are possibly not efficiently dissociated or ionized at low temperatures. At higher forward power settings however they showed an increase in sensitivity due to more efficient sampling. Elements with high first IEs ( $^{66}\text{Zn}$ ,  $^{75}\text{As}$ ,  $^{80}\text{Se}$ , and  $^{128}\text{Te}$ ) form the third group, which shows the highest sensitivity for the highest power and lowest gas flow settings. Detection of these elements merely benefits from a higher temperature increasing the ion yield rather than less diffusion. An exception in this respect was  $^9\text{Be}^+$ , which also has a high first IE, but due to its low mass it also benefits from higher sampling efficiency at a higher flow rate and thus resembled more the trends observed for group 2. Similarly, some contour plots show a trend that is in between group 2 and group 3, namely those of the elements  $^{66}\text{Zn}^+$ ,  $^{111}\text{Cd}^+$ , and  $^{232}\text{Th}^+$ , which have been assigned to the group they are closest to.

The contour plot of  $^{40}\text{Ca}^+$  showed a bimodal distribution which can be seen in Fig. 3. The locations of the two maxima correspond to an element of the first group (high flow and low power), which is considered to be due to  $^{40}\text{Ca}^+$  with its low first IE and an element of the third group, which is most likely caused by residual argon in the plasma gas. This is further supported by the occurrence of the other argon isotopes in a blank sample and the knowledge that standard-grade nitrogen from a conventional cryogenic air distillation may contain up to 0.5% of argon.<sup>34</sup>

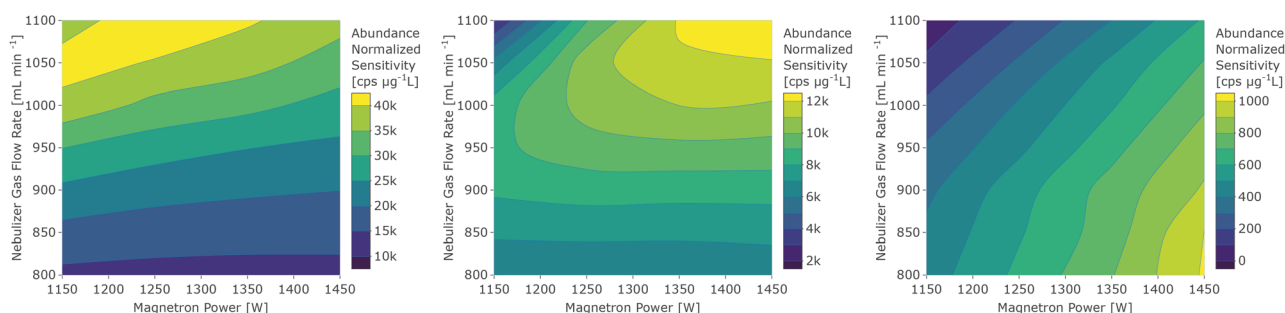
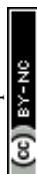


Fig. 2 The abundance normalized sensitivity of an analyte is shown in dependence of the operating power and the nebulizer gas flow rate as contour plots. Three different behaviours exist and are represented with  $^{133}\text{Cs}$  (left),  $^{59}\text{Co}$  (middle) and  $^{75}\text{As}$  (right), measured in the standard interface & additional pump configuration.





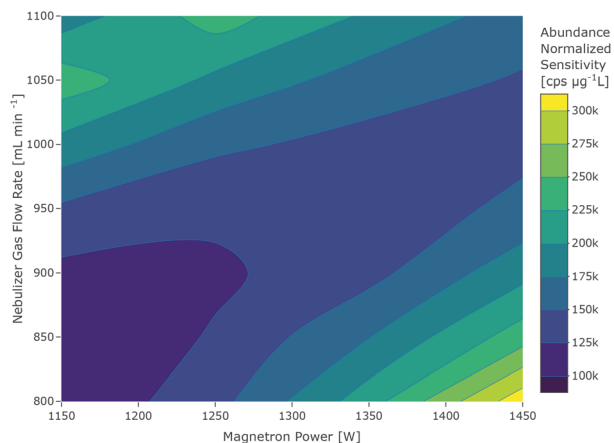


Fig. 3 The operating power vs. gas flow rate contour plot shows two maxima for the sensitivity of  $^{40}\text{Ca}$  in the standard interface & pump configuration, which can be accounted to an argon interference at high operating powers and low gas flow rates and the actual calcium at low operating powers and high gas flow rates.

**Plasma background ions, nitrides, and oxides.** The signals of the monitored plasma background ions mimic the trends observed for analytes with a high first IE; the signals decrease with increasing gas flow rates and decreasing forward power (Fig. S6†). The formation of metal oxide ions however was found to mimic the trend observed in conventional Ar-based ICPs but with slightly higher abundances, indicating an overall lower temperature in the nitrogen plasma. Abundances of the oxide species increased when the plasma temperature was lowered, either by an increase in gas flow rate or a decreased forward power, as can be seen in Fig. S7.† Similar to Ar-based polyatomic ions formed from compounds dissolved in the sample, their counterparts are formed in the  $\text{N}_2$  plasma. Abundance ratios close to 0.5% were observed for  $^{232}\text{Th}^{14}\text{N}^+$  and  $^{238}\text{U}^{14}\text{N}^+$ , but they did not vary substantially when changing the operating conditions. However, the abundance of  $^{140}\text{Ce}^{14}\text{N}^+$  seemed to increase when using gas flow rates higher than  $1 \text{ L min}^{-1}$

(Fig. S8†). Still, due to the low occurrence of nitrides under all conditions, they were not considered relevant for the determination of the most suitable operating conditions.

**Response curves.** To evaluate the most suitable plasma operating conditions, the response curves at  $1150 \text{ W}$  &  $1050 \text{ mL min}^{-1}$ , at  $1450 \text{ W}$  &  $1100 \text{ mL min}^{-1}$ , and under the operation conditions of  $1450 \text{ W}$  &  $800 \text{ mL min}^{-1}$ , corresponding to the locations of the three maxima in the power vs. flow rate contour plots and thus to the three groups, were compared (see Fig. 4). While optimum settings for group 1 elements yielded the highest sensitivities for many elements, substantial suppression was observed for elements with a first IE  $\geq 9 \text{ eV}$  ( $^9\text{Be}^+$ ,  $^{66}\text{Zn}^+$ ,  $^{75}\text{As}^+$ ,  $^{80}\text{Se}^+$ ,  $^{111}\text{Cd}^+$ , and  $^{128}\text{Te}^+$ ) and elements forming refractory oxides ( $^{140}\text{Ce}^+$ ,  $^{232}\text{Th}^+$ , and  $^{238}\text{U}^+$ ). Optimum conditions for group 2 elements alleviated the suppression of the latter, while retaining a high sensitivity for most monitored isotopes. The smallest deviation of sensitivities for elements of similar mass was obtained for optimal settings for group 3 elements but at a substantial loss in sensitivity for the other elements. Operating the ion source with a higher nebulizer gas flow rate reduced the analyte loss caused by diffusion, but the shorter residence time and lower plasma temperature do not allow for efficient dissociation of refractory oxides and ionization of high IE elements. In fact, the oxide abundances were excessively high (18%  $^{140}\text{Ce}^{16}\text{O}^+$ , 44%  $^{232}\text{Th}^{16}\text{O}^+$ , and 19%  $^{238}\text{U}^{16}\text{O}^+$ ) for operating conditions of group 2 elements when compared to the oxide abundances using the operating conditions of group 3 (2.5%  $^{140}\text{Ce}^{16}\text{O}^+$ , 8.6%  $^{232}\text{Th}^{16}\text{O}^+$ , and 3.3%  $^{238}\text{U}^{16}\text{O}^+$ ). Therefore, a compromise between the higher analyte sensitivities (high gas flow) as seen in the response curve of group 2 and the low oxide ratio (low gas flow) corresponding to the response curve of group 3 elements should yield suitable operating conditions.

Based on our experience, the response curve for group 3 most closely resembles the characteristics of the Ar ICP with the same MS. However, even for these settings, the sensitivity of elements with first IE  $\geq 9 \text{ eV}$  appeared to be suppressed to a greater extent in the MICAP source. Specifically  $^{75}\text{As}^+$  and  $^{80}\text{Se}^+$

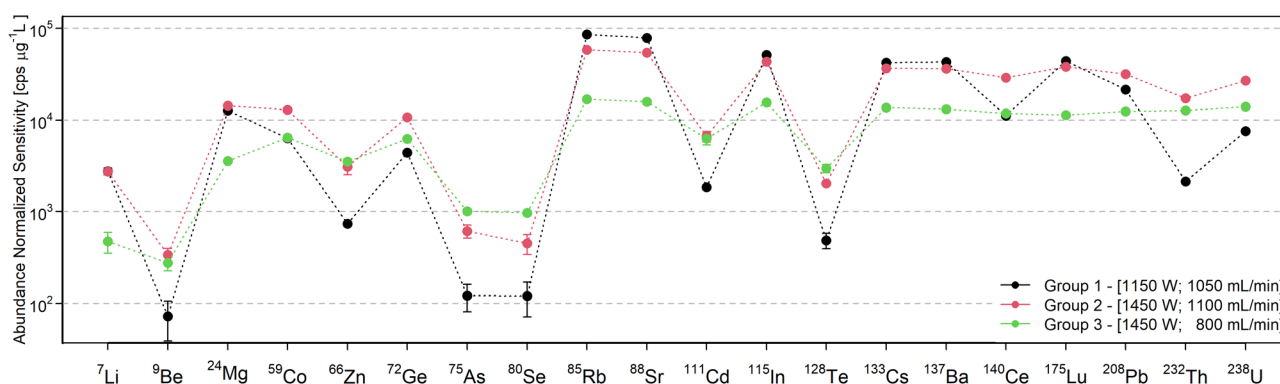


Fig. 4 Response curves of the optimal plasma operating conditions according to the three types of sensitivity behaviours seen in the contour plots. Measurements were performed with the standard interface & pump configuration. The operating conditions corresponding to the three analyte groups are given. The error bars represent two times the standard deviation and are only visible for some elements. (All lines are to guide the eye.)



were detected at more than one order of magnitude lower sensitivities than isotopes of similar mass and lower IEs, which was not the case in an Ar ICP. This is considered to be the result of the high abundance of NO in the plasma source, whose IE (9.264 eV) is close to that of these elements.<sup>33</sup>

## Interface modifications

The evaluation of plasma operating conditions as described above was repeated for six additional interface configurations as listed in Table 1. The observed trends in the isotopes' responses were highly similar with the exception of the  $^{40}\text{Ca}^+$ ,  $^{80}\text{Se}^+$ , and  $^{14}\text{N}_4^+$  trends present in some configurations.

**Interface pressure.** As expected, the interface pressure was reduced by almost 30% when a sampler cone with a smaller orifice was employed. A second interface pump not only decreased the interface pressure by almost 50% but also reduced its increase with higher nebulizer gas flow rates (Fig. S2†). The skimmer position did not significantly change the interface pressure or its flow dependence.

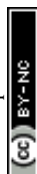
**$^{40}\text{Ca}^+$  trend.** As already mentioned, the contour plot of  $^{40}\text{Ca}^+$  showed a bimodal distribution for the standard interface and pump configuration. However, when using the smaller sampler cone only the peak at low operating powers and high gas flows was observed. The second maximum at high power and low gas flows, which is considered to be from  $^{40}\text{Ar}^+$ , was substantially reduced as can be seen in Fig. S9.† This may be the result of an overall lower sampled plasma temperature, which is supported by an increase in the oxide ratios.

**$^{80}\text{Se}^+$  trend.** When using a setup with the skimmer position further upstream and operating at a high forward power of 1450 W and low to intermediate nebulizer gas flows, the ion signal measured for  $^{80}\text{Se}^+$  increased substantially. Since the  $^{75}\text{As}^+$  signals did not change in the same manner (Fig. S10 left†), this increase is unlikely to be caused by a more efficient ionization of elements with a high IE. The enhancement is thus most likely due to an increased abundance of a spectral interference. Furthermore, this enhancement was higher for the 1 mm skimmer shift than for the 0.5 mm shift. The signal was reduced when higher gas flow rates or a smaller sampler orifice was employed. Lowering the interface pressure with the additional pump also caused a notable suppression but not to the same extent (Fig. S10 right†). The origin of this interference is not clear yet, however, it appears to be related to a molecular ion that is also observed at  $m/z$  82. Both interferences ( $m/z$  80 and 82) have previously been observed with the standard interface for a dry plasma when laser ablation was employed.<sup>28</sup> As they are present for wet and dry sample introduction systems, the water in the wet plasma is an unlikely origin. Together with the observation that these species were only abundant when the plasma was operated at higher temperatures, a formation directly by the plasma gas is likely. Their reduction observed when lowering the interface pressure and employing a reduced sampler cone additionally points towards their abundance being higher in the outer part of the plasma's central channel, as a lower interface pressure increases the radial expansion.

Their identity is however still unknown; the most likely candidates are nitrogen clusters containing carbon and oxygen.

**$^{14}\text{N}_4^+$  trend.** With the skimmer shifted upstream,  $\text{N}_4^+$  intensities were sometimes found to increase with higher gas flow rates, while the other monitored plasma background ions exhibited the same decreasing trend (Fig. S11†). This change was observed when the skimmer shift was combined with either the additional pump (both skimmer shifts) or with the reduced sampler cone (1 mm shift, with and without the pump). In contrast to  $m/z$  80, we consider it unlikely that this is caused by additional molecular ions formed or detected only under these conditions. Formation of  $^{40}\text{Ar}^{16}\text{O}^+$  or  $^{40}\text{Ca}^{16}\text{O}^+$  can be ruled out considering the ion signals measured at  $m/z$  40. It thus appears that  $\text{N}_4^+$  is increasingly sampled or formed through collisions within the interface with the skimmer shifted upstream and a lower interface pressure.

**Response curves.** The seven different interface configurations are compared in Fig. S12† with their response curves and their oxide ratios to determine the most suitable interface configuration. The response curves were obtained for operating conditions that yielded the highest sensitivities while maintaining the  $^{140}\text{Ce}^{16}\text{O}^+$  abundance ratio at or below 3%. Thus, settings resembling the optimum conditions for group 3 elements were chosen, namely the highest possible power (1450 W) and a low nebulizer gas flow (800 mL min<sup>-1</sup> or 850 mL min<sup>-1</sup>). When using the reduced sampler or the skimmer shifted upstream together with the additional pump, however, the  $^{140}\text{Ce}^{16}\text{O}^+$  abundance ratio remained higher than 3% for all employed operating conditions. The depicted response curves appeared all very similar to that of the standard interface. It can be seen that moving the skimmer upstream in all cases led to a lower sensitivity. A slight increase in the response except for  $^7\text{Li}^+$  and  $^9\text{Be}^+$  was obtained when using the standard interface with the second interface pump, which can be explained by the higher gas flow rate that could be employed to maintain the  $^{140}\text{Ce}^{16}\text{O}^+$  abundance ratio at or below 3% (850 mL min<sup>-1</sup> instead of 800 mL min<sup>-1</sup>). When a smaller sampler aperture was used however, the metal oxide abundances increased despite the lower interface pressure, which is currently assumed to be caused by a smaller fraction of the hotter outer region of the central channel being sampled. When the additional pump was used in combination with a skimmer shift, the abundance of  $^{140}\text{Ce}^{16}\text{O}^+$  also increased. The more upstream position of the skimmer may result in the sampling of a larger fraction of the outer region of the still expanding plasma inside the interface, which could explain the lower oxide abundance with the single pump. Further lowering the interface pressure however will lead to a wider radial expansion of the plasma inside the interface, which again reduces the fraction of the hotter outside part of the central channel being sampled. It is currently unclear why the additional pump reduced the  $^{140}\text{Ce}^{16}\text{O}^+$  abundance when using the standard sampler. In any case, shifting the skimmer upstream resulted in no substantial advantage in sensitivity at low gas flow rates; sensitivities for the 0.5 mm (one spacer) and the 1.0 mm shifted (two spacers) skimmer were lower in all cases, implying that they would need a higher gas flow rate and thus an increased ion transmission to be more comparable to



the standard interface. On the other hand, the use of a second interface pump proved beneficial in terms of the oxide ratio, allowing a higher gas flow to be employed. The reduced argon interference when using a smaller sampler cone orifice is generally not advantageous due to the increased oxide formation. Nonetheless, the sensitivities of the standard configuration indicate that no major change in the interface geometry is needed when measuring under wet plasma conditions.

### Limits of detection

The determined LODs of the MICAP are compared with those from previous reports using nitrogen-based MIPs for aqueous solutions.<sup>21,22,35</sup> Additionally, the LODs are compared to those from an Ar-based ICPMS, comprising the same vacuum interface, ion optics and mass analyser as in our laboratory (see Table 2). A comprehensive summary including the blank standard deviations and the analyte sensitivities can be found in the ESI (Table S2†).

While the LODs of the microwave induced nitrogen discharge at atmospheric pressure plasma (MINDAP) and of the moderate power MIP are in the ng mL<sup>-1</sup> range, the detection limits of MICAP and other high-power MIPs are in the range of pg mL<sup>-1</sup>, making them comparable to the Ar-based ICPMS used here. The higher LOD for <sup>7</sup>Li<sup>+</sup> with the MICAP source may be due to the specific optimization of the instrument, while the detection of <sup>40</sup>Ca<sup>+</sup> is affected by substantial background signals from <sup>40</sup>Ar<sup>+</sup> in the MICAP case. <sup>80</sup>Se<sup>+</sup> on the other hand appears to be affected by a not identified molecular ion, causing an elevated background signal. Okamoto<sup>23</sup> reported the preliminary detection limits of a nitrogen MIP for <sup>39</sup>K<sup>+</sup>, <sup>40</sup>Ca<sup>+</sup>, <sup>52</sup>Cr<sup>+</sup>, and <sup>56</sup>Fe<sup>+</sup> to be below 5 pg mL<sup>-1</sup> which are even lower than the ones reported here. The difference in LOD of <sup>56</sup>Fe<sup>+</sup> might be the result of a higher abundance of <sup>14</sup>N<sub>4</sub><sup>+</sup>. Furthermore, the LODs reported here are well comparable with those found in the other solution nebulization MICAP QMS study.<sup>27</sup> Nonetheless, it could be shown that the MICAP has comparable limits of detection to those of an argon ICP coupled to the same mass spectrometer.

**Table 2** Comparison of limits of detection given in ng mL<sup>-1</sup> for earlier nitrogen-sustained MIPs as well as a commercial Ar ICP

| Element | Isotope | MINDAP <sup>21</sup> | MP MIP <sup>22</sup> | HP MIP <sup>35</sup> | MICAP | Ar ICP             |
|---------|---------|----------------------|----------------------|----------------------|-------|--------------------|
| Li      | 7       | —                    | 0.4                  | 0.0004               | 0.03  | 0.004              |
| Mg      | 24      | —                    | 0.4                  | 0.002                | 0.002 | 0.013              |
| Ca      | 40      | 22                   | 0.24                 | 0.014                | 0.05  | —                  |
| V       | 51      | —                    | 0.3                  | 0.001                | 0.001 | 0.003              |
| Cr      | 52      | —                    | 0.4                  | 0.001                | 0.001 | 0.02               |
| Mn      | 55      | —                    | 0.5                  | 0.001                | 0.001 | 0.02               |
| Fe      | 56      | —                    | 7                    | 0.008                | 0.017 | —                  |
| Co      | 59      | 10                   | 0.17                 | 0.001                | 0.002 | 0.002              |
| As      | 75      | —                    | 0.3                  | 0.02                 | 0.012 | 0.009              |
| Se      | 80      | —                    | 1.4                  | 0.04                 | 0.08  | —                  |
| Sr      | 88      | 3                    | 0.4                  | 0.002                | 0.002 | 0.002              |
| Ba      | 138     | 11                   | 0.3                  | 0.004                | 0.001 | 0.003 <sup>a</sup> |
| Pb      | 208     | —                    | 6                    | 0.008                | 0.001 | 0.002              |

<sup>a</sup> Measured <sup>137</sup>Ba.

## Conclusions

The investigation of the characteristics of the novel high-power nitrogen-sustained microwave inductively coupled atmospheric pressure plasma as the ion source for element mass spectrometry has revealed the following main findings:

The change in the plasma gas temperature could be estimated through the interface pressure changes, showing a 2–4% lower plasma temperature with increasing the nebulizer gas flow rate by 100 mL min<sup>-1</sup> or decreasing the microwave power by 100 W. The influence of the operating conditions on analyte sensitivity has been assessed by varying the forward power and the nebulizer gas flow rate, which indicate that the monitored elements could be divided into three groups based on the location of their maximum sensitivity, which can be related to their respective physical-chemical properties such as mass, first IE, and oxygen bond strength. The signals of the investigated plasma background ions were found to mimic the trends observed for analytes with a high IE, as the signal decreased with increasing gas flow rates and decreasing forward power. The metal oxide ions followed the trends observed in the conventional argon-based ICP, but their abundances were slightly higher, indicating an overall lower temperature in the nitrogen plasma. On the other hand, the observed nitride abundances were near 0.5% and seemed to be mostly independent from the operating conditions. Based on these observations and a comparison of response curves under different operating conditions, it can be recommended to operate the MICAP ion source at a high power and a low flow rate to maintain a low abundance of oxides while also reducing the relative suppression of high IE elements.

The influence of different interface variations including a smaller sampler aperture, shortening the sampler-skimmer distance, and the use of a second interface pump was evaluated. The use of a smaller sampler orifice appears to result in sampling from a colder plasma region since the oxide ratios were higher and the <sup>40</sup>Ar ion signal was less abundant. Shifting the skimmer position further upstream led to a decrease in the analyte sensitivity and oxide ratios with decreasing sampler-skimmer distance. Additionally, the ion signal at *m/z* 80 and 82 increased when the skimmer was shifted further upstream and the plasma was operated at higher temperatures, which originates from a yet unknown interference. In any case, no substantial advantage in sensitivity was observed by shortening the sampler-skimmer distance or using a smaller sampler orifice. A slight increase in the response was obtained when using the standard interface with the second interface pump, which allowed a higher nebulizer gas flow rate to be used while maintaining a low metal oxide abundance level. Nonetheless, this study shows that the ion source can be operated under conditions that result in only slightly lower analyte sensitivities compared to an Ar-based ICP, a comparable abundance of metal oxides and negligible amounts of nitrides, even for the standard configuration, indicating that no major change in the interface geometry is needed when introducing wet aerosols.

The performance of the MICAP ion source was further evaluated by calculating the LODs, which were found to be



comparable to those of other nitrogen sustained MIPs as well as to an argon-based ICP instrument, using the same ion optics and mass spectrometer. Considering all these findings and the operating cost of the MICAP source, it has proven to be a complementary or even competitive ion source for element mass spectrometry.

## Conflicts of interest

The authors declare that they have no known competing financial interests or personal relationships that could have appeared to influence the work reported in this paper.

## Acknowledgements

Special thanks go to Ashok Menon and Jovan Jevtic of Radom Corporation and Philippe Trüssel from the DCHAB central workshop for their assistance and to the Swiss National Science Foundation for their financial support through project number 200021\_197224.

## References

- 1 R. S. Houk, *Anal. Chem.*, 1980, **52**, 2283–2289.
- 2 A. Montaser, *Inductively Coupled Plasma Mass Spectrometry*, Wiley-VCH, New York, 1998.
- 3 L. Hendriks, A. Gundlach-Graham, B. Hattendorf and D. Günther, *J. Anal. At. Spectrom.*, 2017, **32**, 548–561.
- 4 A. L. Gray, *Analyst*, 1985, **110**, 551–556.
- 5 D. Günther and B. Hattendorf, *TrAC, Trends Anal. Chem.*, 2005, **24**, 255–265.
- 6 A. Prange and D. Pröfrock, *Anal. Bioanal. Chem.*, 2005, **383**, 372–389.
- 7 M. Montes-Bayon, D. Pröfrock, A. Sanz-Medel and A. Prange, *J. Chromatogr. A*, 2006, **1114**, 138–144.
- 8 E. Krupp, F. Seby, R. Rodríguez Martín-Doimeadios, A. Holliday, M. Moldován, G. Köllensperger, S. Hann and O. F. X. Donard, in *Inductively Coupled Plasma Mass Spectrometry Handbook*, Blackwell Publishing Ltd., 2009, pp. 259–335.
- 9 D. J. Douglas and J. B. French, *J. Anal. At. Spectrom.*, 1988, **3**, 743–748.
- 10 S. Elliott, M. Knowles and I. Kalinitchenko, *Spectroscopy*, 2004, **19**, 30–38.
- 11 I. Feldmann, N. Jakubowski and D. Stuewer, *Fresenius. J. Anal. Chem.*, 1999, **365**, 415–421.
- 12 S. D. Tanner and V. I. Baranov, *At. Spectrosc.*, 1999, **20**, 45–52.
- 13 B. Hattendorf and D. Günther, *J. Anal. At. Spectrom.*, 2000, **15**, 1125–1131.
- 14 D. P. Myers and G. M. Hieftje, *Microchem. J.*, 1993, **48**, 259–277.
- 15 I. Feldmann, W. Tittes, N. Jakubowski, D. Stuewer and U. Giessmann, *J. Anal. At. Spectrom.*, 1994, **9**, 1007–1014.
- 16 O. Borovinskaya, B. Hattendorf, M. Tanner, S. Gschwind and D. Günther, *J. Anal. At. Spectrom.*, 2013, **28**, 226–233.
- 17 S. Greenfield, I. L. Jones, C. T. Berry and J. M. Mermet, *J. Anal. At. Spectrom.*, 1964, **4**, 559–560.
- 18 R. H. Wendt and V. A. Fassel, *Anal. Chem.*, 1965, **37**, 920–922.
- 19 C. I. M. Beenakker, *Spectrochim. Acta, Part B*, 1976, **31**, 483–486.
- 20 Y. Okamoto, M. Yasuda and S. Murayama, *Jpn. J. Appl. Phys., Part 1*, 1990, **29**, L670–L672.
- 21 D. A. Wilson, G. M. Hieftje and G. H. Vickers, *Anal. Chem.*, 1987, **59**, 1664–1670.
- 22 W.-L. Shen, T. M. Davidson, J. T. Creed and J. A. Caruso, *Appl. Spectrosc.*, 1990, **44**, 1003–1010.
- 23 Y. Okamoto, *J. Anal. At. Spectrom.*, 1994, **9**, 745–749.
- 24 J. Jevtic, A. Menon and V. Pikelja, *U.S. Pat.*, WO 2014/159588 A1, 2014.
- 25 A. J. Schwartz, Y. Cheung, J. Jevtic, V. Pikelja, A. Menon, S. J. Ray and G. M. Hieftje, *J. Anal. At. Spectrom.*, 2016, **31**, 440–449.
- 26 M. Schild, A. Gundlach-Graham, A. Menon, J. Jevtic, V. Pikelja, M. Tanner, B. Hattendorf and D. Günther, *Anal. Chem.*, 2018, **90**, 13443–13450.
- 27 Z. You, A. Akkuş, W. Weisheit, T. Giray, S. Penk, S. Buttler, S. Recknagel and C. Abad, *J. Anal. At. Spectrom.*, 2022, **37**, 2556–2562.
- 28 C. Neff, P. Becker, B. Hattendorf and D. Günther, *J. Anal. At. Spectrom.*, 2021, **36**, 1750–1757.
- 29 J. E. Fulford and D. J. Douglas, *Appl. Spectrosc.*, 1986, **40**, 971–974.
- 30 R. S. Houk, *Anal. Chem.*, 1986, **58**, 97A–105A.
- 31 S. Gschwind, L. Flamigni, J. Koch, O. Borovinskaya, S. Groh, K. Niemax and D. Günther, *J. Anal. At. Spectrom.*, 2011, **26**, 1166–1174.
- 32 L. Flamigni, J. Koch and D. Günther, *J. Anal. At. Spectrom.*, 2014, **29**, 280–286.
- 33 *CRC Handbook of Chemistry and Physics*, ed. J. Rumble, CRC Press, Boca Raton, FL, 102nd edn, 2021.
- 34 R. Agrawal, *Ind. Eng. Chem. Res.*, 1996, **35**, 1059–1071.
- 35 K. Oishi, T. Okumoto, T. Iino, M. Koga, T. Shirasaki and N. Furuta, *Spectrochim. Acta, Part B*, 1994, **49**, 901–914.

